

Statistical downscaling of daily mean temperature, pan evaporation and precipitation for climate change scenarios in Haihe River, China

J. T. Chu · J. Xia · C.-Y. Xu · V. P. Singh

Received: 9 September 2008 / Accepted: 4 March 2009 / Published online: 24 April 2009
© Springer-Verlag 2009

Abstract A statistical downscaling method (SDSM) was evaluated by simultaneously downscaling air temperature, evaporation, and precipitation in Haihe River basin, China. The data used for evaluation were large-scale atmospheric data encompassing daily NCEP/NCAR reanalysis data and the daily mean climate model results for scenarios A2 and B2 of the HadCM3 model. Selected as climate variables for downscaling were measured daily mean air temperature, pan evaporation, and precipitation data (1961–2000) from 11 weather stations in the Haihe River basin. The results obtained from SDSM showed that: (1) the pattern of change in and numerical values of the climate variables can be reasonably simulated, with the coefficients of determination between observed and downscaled mean temperature, pan evaporation, and precipitation being 99%, 93%, and 73%, respectively; (2) systematic errors existed in simulating extreme events, but the results were acceptable for practical

applications; and (3) the mean air temperature would increase by about 0.7°C during 2011–2040; the total annual precipitation would decrease by about 7% in A2 scenario but increase by about 4% in B2 scenario; and there were no apparent changes in pan evaporation. It was concluded that in the next 30 years, climate would be warmer and drier, extreme events could be more intense, and autumn might be the most distinct season among all the changes.

1 Introduction

Increasing concentration of CO₂ and other greenhouse gases, along with intensifying human activities, are perturbing the global energy balance, heating up atmosphere, and causing global warming (Xu 1999; Wentz et al 2007). It has been pointed out in the fourth report of the Intergovernmental Panel on Climate Change (IPCC) that the global surface temperature has increased by 0.74°C in the latest century (1906–2005), and the increasing rate is about 0.13°C/10 years in the past 50 years; this report also predicted that surface temperature would continue to increase at a rate of 0.2°C/10 years in the next 20 years and would increase by about 1.1–6.4°C during the next century (IPCC 2007). Global warming will disturb the worldwide water cycle; in turn, the changed hydrological regime will affect nearly every aspect of human activities, such as fish management and health of ecosystems, industrial and municipal water supply, water energy exploitation, human health, etc.

The state-of-art General Circulation Models (GCMs) can reproduce important processes about global- and continental-scale atmosphere and predict future climate under different emission scenarios. Although there are many uncertainties in different GCMs, they are still the most adapted approach, to

J. T. Chu (✉) · J. Xia
Key Laboratory of Water Cycle & Related Land Surface Processes, Institute of Geographic Sciences and Natural Resources Research, Chinese Academy of Sciences, Beijing 100101, China
e-mail: cjtqd@yahoo.com.cn
e-mail: chujt.06b@igsnr.ac.cn

J. T. Chu
Graduate University of the Chinese Academy of Sciences, Beijing 100039, China

C.-Y. Xu
Department of Geosciences, University of Oslo, P. O. Box 1047 Blindern, NO-0316 Oslo, Norway

V. P. Singh
Department of Biological and Agricultural Engineering, Texas A & M University, Scoates Hall, 2117 TAMU, College Station, TX, USA

date, to obtain information on climate change. Since spatial resolutions of GCMs are often coarse (hundreds of kilometer), there is a mismatch of scale between GCMs and the scale of interest for regional impacts (an order or two orders of magnitude finer scale). For many regional and local applications, users of climate model results have long been dissatisfied with the inadequate spatial scale of climate scenarios produced from coarse resolution GCMs outputs (Cubasch et al. 1996; Risbey and Stone 1996; Eric and Salathe 2003). In the past couple of decades, different downscaling methods have been proposed in order to deal with the problem of spatial scale mismatch, and these methods have been widely used in their cradles, such as Europe and USA (Hanssen-Bauer et al. 2005; Fowler and Wilby 2007; Hellstrom et al. 2001; Wilks 1989; Murphy 2000; Hayhoe et al. 2004; Vrac et al. 2007; Coulibaly 2004; Wetterhall et al. 2005, 2006, 2007).

Downscaling methods can be broadly divided into two classes: dynamical downscaling (DD) and statistical (empirical) downscaling (SD). In DD, the GCM outputs are used as boundary conditions to drive a Regional Climate Model or Limited Area Model and produce regional-scale information up to 5~50 km. This method has superior capability in complex terrain or with changed land cover (Wang et al. 2004; Kite 1997). However, this method entails higher computation cost and relies strongly on the boundary conditions provided by GCMs. In contrast, SD gains local- or station-scale meteorological time series (predictands) by appropriate statistical or empirical relationships with surface or troposphere atmospheric features (predictors; Xu 1999; Wilby and Wigley 1997; Fowler et al. 2007). Since this method is inexpensive to use and is as powerful as its dynamic competitor, it has been widely employed in climate change impact assessments. However, its drawback is that it needs much longer historical time series to build the appropriate statistical relationship. In addition, one of the assumptions of SD, which is the built statistical relationship, is still valid in the future; this assumption cannot be tested at present.

According to techniques for application, SD methods can be classified into three categories: regression methods (Von Storch et al. 1993; Kang et al. 2007; Burger and Chen 2005); weather pattern-based approaches (Bardossy and Plate 1992); and stochastic weather generators (Richardson 1981). No matter whether the method is simple or complex, it is always based on some kind of a regression relationship. Regression methods depend on linear or nonlinear relationships between predictands and predictors. Nowadays, many regression methods, such as Artificial Neural Networks (Tripathi et al. 2006), Multiple Linear Regression (MLR), Canonical Correlation Analysis (Busuioc et al. 1999; Frias et al. 2006), and Principal Component Analysis, have been widely used in the hydrologic response assessment. SDSM

is a hybrid of a regression method and weather generator (Wilby et al. 1999, 2002, 2003). Many comparative studies (Fowler et al. 2007; Wilby et al. 1998; Khan et al. 2006; Harpham and Wilby 2005; Dibike and Coulibaly 2005) have shown that this method is simple to handle and has, by and large, superior capability and is, therefore, widely applied (Wilby and Harris 2006).

In China, statistical downscaling methods have gradually started to receive increasing attention (Fan 2006; Yuan et al. 2005; Fan et al. 2005, 2007; Chen and Chen 2001; Chen et al. 2006; Liao et al. 2004). When compared with western countries, studies on downscaling have, however, been meager, and most of these studies are limited to daily precipitation using a weather generator method (Liao et al. 2004). SDSM has once been used in the upper and middle reaches of the Yellow River Basin, China (Zhao and Xu 2008; Liu et al. 2008) and has mainly focused on maximum and minimum temperatures as well as precipitation. Simultaneously downscaling of precipitation, temperature, and evaporation has not been reported elsewhere at present.

The objective of this article, therefore, is twofold: (1) to investigate the adaptability of SDSM for simultaneously downscaling mean temperature, pan evaporation, and precipitation in Haihe River basin and discuss strengths and weaknesses of the method when applied to semiarid regions in China; (2) to provide local-scale climate change information under future emission scenarios, which will be used in the ongoing research on water resources assessment under future climate change. To the best of our knowledge, such study has not been reported at least for Chinese regions. This study may be a valuable reference for many others who are going to apply SDSM to other regions of China and also provide valuable database for future climate change scenarios in the Haihe River basin covering Beijing and several other large cities and economic regions.

2 Study area and data

2.1 Study area

The Haihe River basin, located between 112–120° E and 35–43° N, has a total area of about 31.8×10^4 km²; 60% of the area is occupied by hills and plateau area, and the remaining 40% is a plain area. To the north of the catchment is the Yan Mountain, to the south is the Taihang Mountain, and to the east of the catchment is the North China plain.

The climate of Haihe River basin ranges from semi-humid and semiarid continental monsoon. It is arid and dry in spring, hot and humid in summer, sunny in autumn, and cold and dry in winter. The multiyear average air temperature gradually rises from northwest to southeast, and multiyear average pan evaporation is between 1,500 and 2,000 mm/

year (Ren 2007). The Haihe River basin has the least rainfall along the east coast of China, with multiyear annual rainfall being about 350–750 mm/year and mainly concentrated in July and August. The spatial distribution of rainfall is also uneven; there is more rain along the coast due to strong sea–land wind or along the windward side of the Yan Mountain and Taihang Mountain affected by orographic uplift. However, rainfall on the leeward side is obviously less than that on the windward side because mountains obstruct the water vapor and make the airflow sink down (Shi 1995).

Mean temperature, pan evaporation, and precipitation are the important climate parameters (Fan and Liu 1992). The migration of rain belts, as well as the change of tempo-spatial distribution and intensity of precipitation, has a direct influence on the total amount of water resources, while temperature and pan evaporation can indirectly affect the hydrologic trend due to the interaction with land surface processes on a longer time scale.

The basin area was represented as a grid with 3.75° (longitude) \times 2.5° (latitude), which is identical to the HadCM3 resolution. This region centers at 116.25° E and 40° N, i.e., the

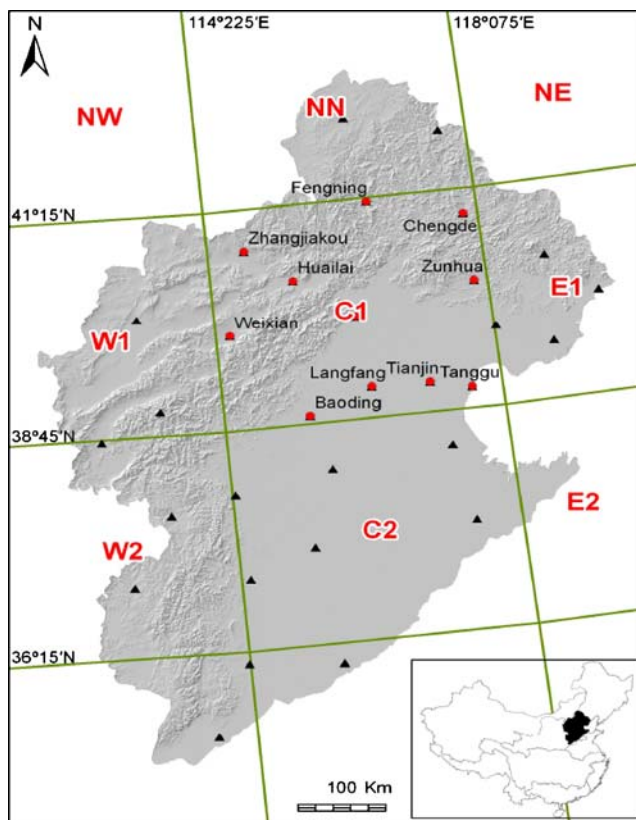


Fig. 1 Location map of weather stations in Haihe River basin, in which, the Haihe River basin has been divided into nine grids by green lines, with the name indicated by red letter; black triangle means 52 weather stations in Haihe River basin; red dot means 11 weather stations in study region—region C1, and black letter indicates the names of weather stations in region C1

region C1 in Fig. 1. Because all of the typical topographies, such as coast, plain, and mountains, are contained in this region, it is a representative area for downscaling studies. There are 11 weather stations in the region C1, including those important cities, such as Beijing, Tianjin, Zhangjiakou, etc. These cities occupy special political and socioeconomic centers in China. In the past decades, groundwater in North China plains has been seriously overexploited, resulting in a wide disparity between water demand and water supply. Consequently, it is of urgent significance to also study how to guarantee sustainable utilization of water resources in these cities under changing environment and increasing uncertainty.

2.2 Data

Measured daily mean air temperature, pan evaporation, and precipitation of 11 weather stations from 1961 to 2000 were selected from the daily observation data of China Meteorological Administration. Since daily pan evaporation data have missing values for some stations, two continuous data periods for pan evaporation, i.e., 1962.1.1–1966.8.31 and 1970.9.1–2000.12.31, were chosen for this study, while for air temperature and precipitation, the complete period from 1961–2000 was used. The basic information about these three predictands can be seen in Table 1.

There are 23 different atmospheric variables, and these were derived from the daily reanalysis dataset of NCEP/NCAR for 1961–2001 at a scale of 2.5° (long.) \times 2.5° (lat.), as well as outputs of scenarios A2 and B2 of HadCM3 from 1961 to 2099, with a spatial resolution of 3.75° (long.) \times 2.5° (lat.; Table 2). First, we interpolated the NCEP data in order to adjust its resolution to the same as scenarios A2 and B2 of HadCM3 model then normalized all of these atmospheric data as:

$$\hat{u}_t = \frac{u_t - \bar{u}}{\sigma_u} \quad (1)$$

in which \hat{u}_t is the normalized atmospheric variable at time t , u_t is the original data at time t , \bar{u} is the multiyear average during the period, and σ_u is the standard deviation. The results can be directly downloaded from the internet using the site: <http://www.cics.uvic.ca/scenarios/sdsm/select.cgi>

3 Methodology

As a first step, a quantitative statistical relationship between large-scale atmospheric variables and local-scale variables was established (Chen 2000) as:

$$Y = F(X) \quad (2)$$

Table 1 Basic information about 11 weather stations in the Region C1

station code	station name	Abbr.	longitude	latitude	altitude <i>m</i>	Mean annual temperature °C	pan evaporation <i>mm/yr</i>	rainfall <i>mm/yr</i>
54405	Huailai	hl	115°30'	40°24'	537	9.5	2124	381
54401	Zhangjiakou	zk	114°53'	40.47'	724	8.6	1933	401
53593	Weixian	wx	114°34'	39°50'	910	6.9	1621	406
54308	Fengning	fn	116°38'	41°13'	660	6.7	1636	467
54518	Langfang	lf	116°23'	39°07'	9	12.1	1776	510
54423	Chengde	cd	117°56'	40°58'	377	9.1	1530	526
54602	Baoding	bd	115°31'	38°51'	17	12.8	1645	533
54527	Tianjin	tj	117°10'	39°06'	3	12.6	1678	547
54511	Beijing	bj	116°17'	39°56'	54	12.2	1841	575
54623	Tanggu	tg	117°43'	39°00'	3	12.5	1969	589
54429	Zunhua	zh	117°57'	40°12'	55	10.8	1607	744
Area-average					304	10.3	1760	516

The time span of mean annual temperature and rainfall is 40 years, which is between 1961.1.1~2000.12.31, while 35 years for pan evaporation, that is, 1962.1.1~1966.8.31 and 1970.9.1~2000.12.31

in which *Y* means the local predictand, $X(x_1, x_2, \dots, x_n)$ represents *n* large-scale atmospheric predictors, and *F* is the built quantitative statistical relationship.

SDSM uses large-scale atmospheric variables to condition the rain occurrence as well as the rainfall amount in wet days. It can be expressed as follows (Wetterhall et al. 2005; Wilby et al. 1999, 2003):

$$\omega_t = \alpha_0 + \sum_{j=1}^n \alpha_j \hat{u}_t^{(j)} + \alpha_{t-1} \omega_{t-1} \tag{3}$$

in which *t* is time (days), ω_t is the conditional possibility of rain occurrence on day *t*, $\hat{u}_t^{(j)}$ is the normalized predictor, α_j is the regression parameter deduced by an ordinary least square method, and ω_{t-1} and α_{t-1} are the conditional probabilities of rain occurrence on day *t*-1 and lag-1 day regression parameters, respectively. These two parameters are optional, depending on the study region and predic-

tand. We used a uniformly distributed random number r_t ($0 \leq r_t \leq 1$) to determine the rain occurrence and supposed that rain would happen if $\omega_t \leq r_t$.

On a wet day, rainfall can be expressed by a z-score as:

$$Z_t = \beta_0 + \sum_{j=1}^n \beta_j \hat{u}_t^{(j)} + \beta_{t-1} + \varepsilon \tag{4}$$

in which Z_t is the z-score on day *t*, β_j is the calculated regression parameter, and β_{t-1} and Z_{t-1} are the regression parameter and the z-score on day *t*-1, respectively. As mentioned above, they are also optional; ε is a random error term represented by the normal distribution $N(0, \sigma_\varepsilon^2)$.

Then, rainfall y_t on day *t* can be written as:

$$y_t = F^{-1}[\phi(Z_t)] \tag{5}$$

in which ϕ is the normal cumulative distribution function and *F* is the empirical distribution function of y_t .

Table 2 The 23 candidates of atmospheric variables for predictors

Variable	Description	Variable	Description
p5_f	Geostrophic airflow velocity at 500 hPa	p8_f	Geostrophic airflow velocity at 850 hPa
p5_u	Horizontal wind at 500 hPa	p8_u	Horizontal wind at 850 hPa
p5_v	Zonal wind at 500 hPa	p8_v	Zonal wind at 850 hPa
p5_z	Vorticity at 500 hPa	p8_z	Vorticity at 850 hPa
p5zh	Divergence at 500 hPa	p8zh	Divergence at 850 hPa
p500	Geopotential height at 500 hPa	p850	Geopotential height at 850 hPa
r500	Relative humidity at 500 hPa	r850	Relative humidity at 850 hPa
p_f	Surface geostrophic airflow	mslp	Mean sea level pressure
p_u	Surface horizontal wind	rhum	Near surface relative humidity
p_v	Surface zonal wind	shum	Near surface specific humidity
p_z	Surface vorticity	temp2	2-m air temperature
p_zh	Surface divergence		

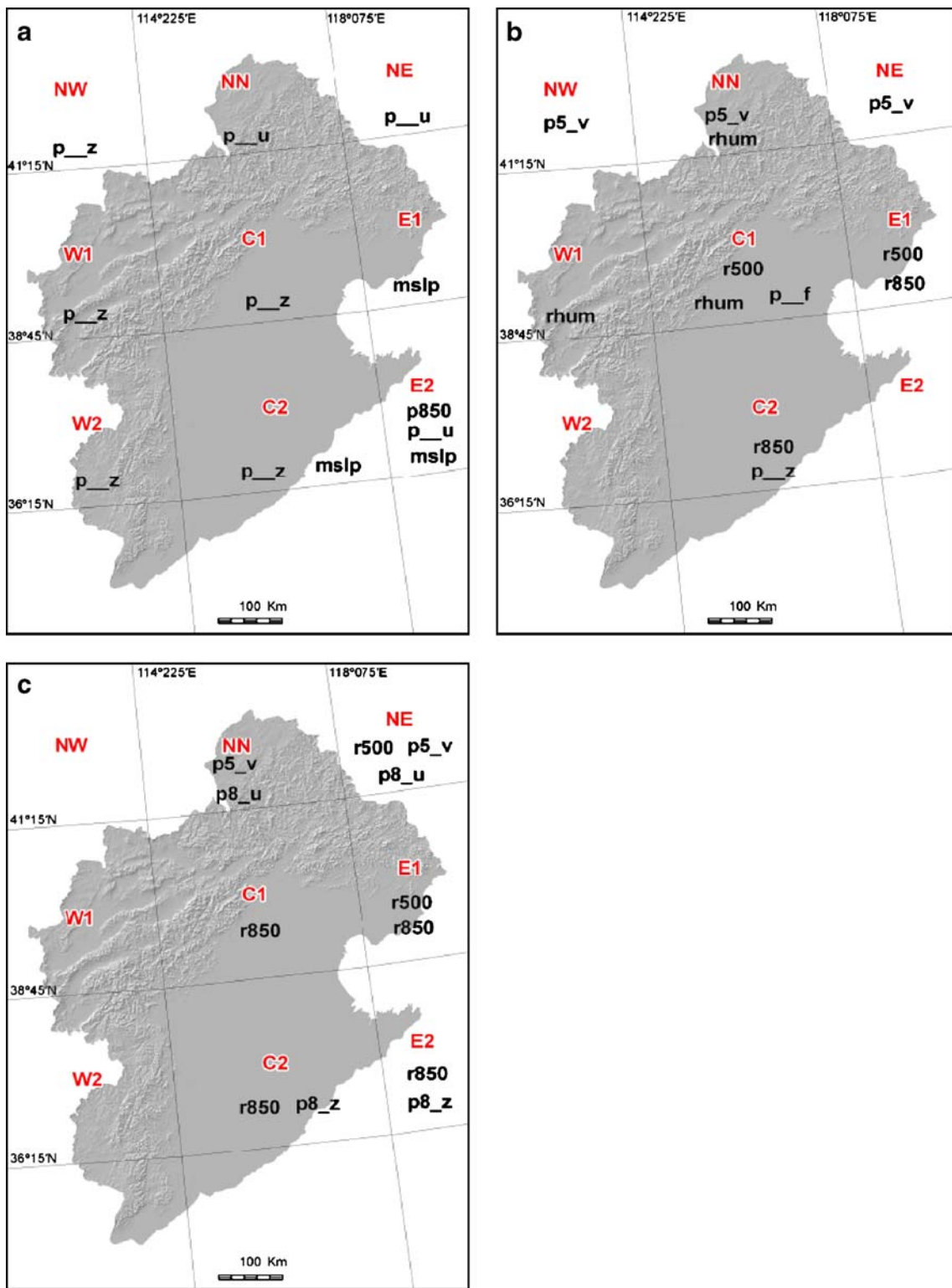


Fig. 2 Predictors (in *black bolds*) and corresponding regions (in *red*) for different predictands; **a** for mean temperature (°C); **b** for pan evaporation (mm); **c** for precipitation (mm). In which, the meaning of predictors are same as in the Table 2

As far as daily temperature and pan evaporation are concerned, we just need to consider the stochastic amount, so Eq. 3 is not needed.

4 Downscaling daily mean temperature, pan evaporation, and precipitation

4.1 Calibration and validation of SDSM

4.1.1 Selecting predictors

The climate in China is strongly controlled by the East Asian monsoon, in which the atmosphere circulation feature is quite different between winter and summer, and the scale of circulation pattern is large. Thus, it is a huge challenge in China to choose predictors in the wide tempo-spatial space (Samel et al. 1999). The procedure adopted in the study for selecting suitable predictors for each predictand is as follows:

First, all of the 23 atmospheric variables in nine regions (region C1 and surrounding eight regions, i.e., NW, NN, NE, W1, E1, W2, C2, and E2) were taken as potential predictors; second, the SMLR method was employed with the confidence level of selection and rejection being 0.001 and the magnitude of probability of every predictor was considered in every region and month; third, the most sensitive regions and predictors for each station month by month were analyzed, and the analysis results of 11 stations was integrated; and finally, 12 predictors were selected for each predictand (Fig. 2).

It is clearly seen that different atmospheric predictors control different local variables: mean temperature is most sensitive to surface and near surface atmospheric factors, and its predictors cover all of the nine regions. In the northwest, surface vorticity and horizontal wind play an important role, while in the southeast, mean sea level pressure is more prominent. As to the pan evaporation, the most relevant predictors occur above 700 hPa. In the north, airflow is horizontally transferred at 500 hPa, while in the middle and southern parts, the predictors are relative humidity at 500 and 850 hPa level. When precipitation is concerned, in the north, the airflow is zonally transferred above 700 hPa while horizontally transferred below 700 hPa; in the southern part, the water vapor is mainly transferred to the north by vorticity at 850 hPa. All of these are similar to the conclusion about the water vapor transmission in the North China deduced by Fan and Liu (1992).

4.1.2 Calibration and validation of SDSM

In this study, the calibration periods for mean temperature and precipitation were 30 years from 1961 to 1983 and

1994 to 2000, and the validation period was 1984–1993. For pan evaporation, the calibration period was 25 years excluding a few years with missing data as mentioned before, that is, 1962.1.1–1966.8.31, 1970.9.1–1983.12.31, and 1994.1.1–2000.12.31. The validation period was the same as for temperature and precipitation.

Taking the selected NCEP reanalysis data as predictors, we built SDSM month by month considering the lag-1 day autoregression. The threshold of wet day was 0 mm. The calibration results are shown in Table 3.

Table 3 shows that the values of μ , C_v , and C_s of simulated air temperature are in good agreement with those of the observed values; at the $\alpha=0.01$ confidence level, the coefficient of determination (R^2) between simulated and observed air temperature at all stations exceeded 99%. The simulated and observed values of μ , C_v , and C_s for

Table 3 Comparison of mean value (μ), coefficient of variation (C_v), coefficient of skewness (C_s), determination coefficient (R^2), and Root Mean Square Error between observed and simulated results for each station in the calibration period (1961–1983 and 1994–2000) and the validation period (1984–1993; $\alpha=0.01$)

	μ	C_v	C_s	R^2	RMSE
Temperature (°C)					
Calibration					
OBS	10.332	1.213	-0.216		
NCEP	10.341	1.211	-0.218	0.9952	0.78
Validation					
OBS	10.397	1.192	-0.22		
NCEP	10.32	1.199	-0.213	0.9974	0.57
H3A2	10.261	1.212	-0.225	0.9692	1.96
H3B2	10.186	1.234	-0.245	0.97	1.95
Evaporation (mm)					
Calibration					
OBS	4.883	0.723	0.874		
NCEP	4.888	0.726	0.8	0.9255	23.34
Validation					
OBS	4.635	0.707	0.737		
NCEP	4.941	0.709	0.76	0.9815	11.49
H3A2	4.712	0.683	0.73	0.8906	24.75
H3B2	4.783	0.69	0.73	0.8645	28.72
Precipitation (mm)					
Calibration					
OBS	1.417	4.528	8.803		
NCEP	1.354	4.354	9.285	0.7296	28.66
Validation					
OBS	1.4	4.293	7.958		
NCEP	1.198	4.453	9.307	0.8949	14.58
H3A2	1.311	3.997	8.264	0.7553	21.34
H3B2	1.277	4.056	8.264	0.7205	22.6

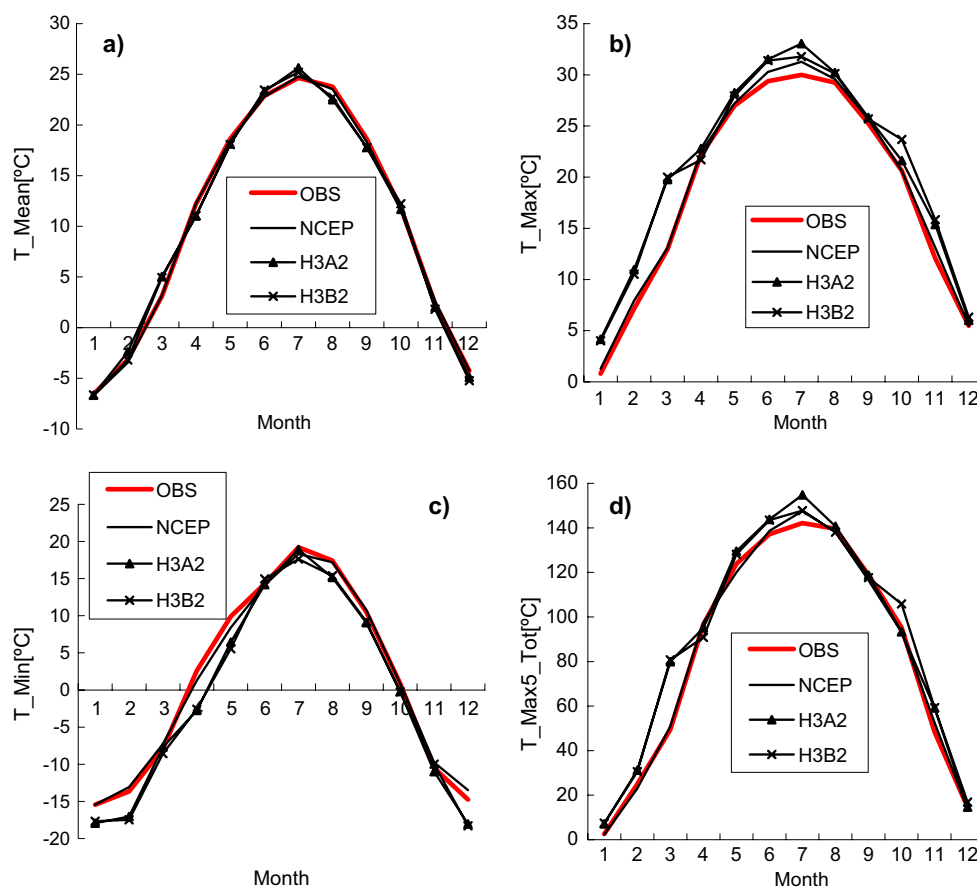


Fig. 3 Comparison of **a** Monthly mean temperature (T_{Mean}), **b** Maximum daily mean temperature (T_{Max}), **c** Minimum daily mean temperature (T_{Min}) and **d** Maximum 5-day continuous cumulative

evaporation were also very similar; the average R^2 value for pan evaporation was around 93%. As to precipitation, its μ value for simulations was slightly lower than that for observations, the difference between simulated and observed C_v and C_s values were in general within 10% except on very few occasions. The R^2 values for the downscaled precipitation were slightly lower than that for the other two predictands; on the average, R^2 was about 73%.

To validate the SDSM method, three sets of atmospheric data were used, i.e., from NCEP, as well as scenario A2 and B2 from HadCM3 model (noted as H3A2 and H3B2, respectively). The results for the validation period are also shown in Table 3. It is seen that the mean temperature was well simulated from NCEP, H3A2, and H3B2 with the R^2 values being up to 97%. However, when downscaling pan evaporation and precipitation, R^2 from NCEP were remarkably better than from H3A2 and H3B2; and H3B2 was a little worse than H3A2. The error was mainly reflected in the high values which might be because SDSM was calibrated with NCEP data; therefore, the built parameters had biases when the model was driven by the H3A2 and H3B2 data. Other statistics, i.e., μ , C_v , and C_s were comparable between downscaled and observed data.

temperature ($T_{\text{Max5_Tot}}$) between observed and generated values in the validation period (1984–1993)

4.2 Comparison of statistical indices of downscaling for the validation period

The preceding section has shown that mean values of all three predictands were well simulated by SDSM; however, extreme climate events, such as droughts, floods, or hot spells, potentially have a much greater impact on water resources management than have average values. Possible future risks under extreme climate have, therefore, been paid more and more attention. It is, therefore, necessary to assess the capacity of SDSM to grasp the features of extreme events. With reference to STARDEX statistical indices, different indicators were employed for different predictands.

4.2.1 Mean temperature

It is seen in Fig. 3 that the pattern of seasonal variation of mean temperature was well downscaled with all three datasets (NCEP, H3A2, H3B2), and the results from NCEP were the best. In simulating the T_{Max} and $T_{\text{Max5_Tot}}$, the results from H3A2 and H3B2 were obviously systematically larger, while in simulating the T_{Min} , the results were lower than observations. The overestimation or

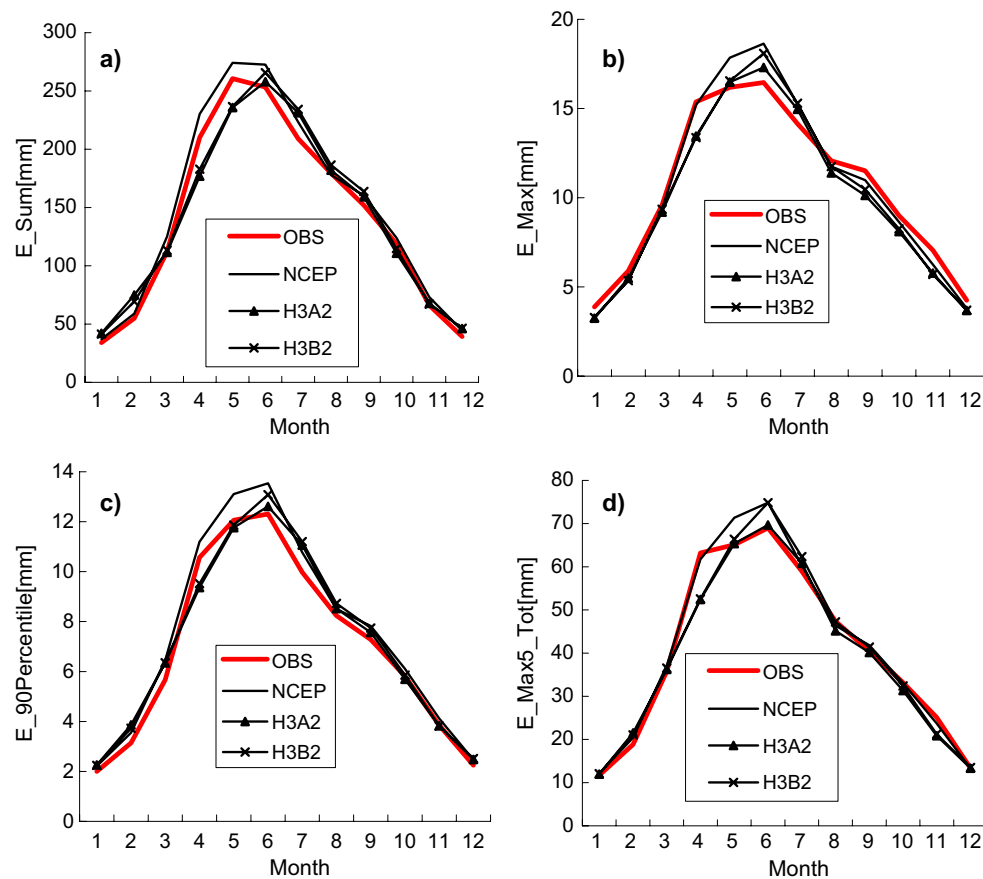


Fig. 4 Comparison of **a** Monthly mean pan evaporation (E_{Sum}), **b** Maximum daily pan evaporation (E_{Max}), **c** 90% quantile of daily pan evaporation ($E_{90Percentile}$) and **d** Maximum 5-day continuous

underestimation was most distinct in April. All of these showed that: (1) the mean value and seasonal variation of mean temperature can be accurately simulated by SDSM fed by NCEP, H3A2, or H3B2 and (2) the T_{Max} was somehow overestimated and T_{Min} was underestimated by the H3A2 and H3B2 data.

4.2.2 Pan evaporation

The results for pan evaporation are shown in Fig. 4. It is seen that in simulating the E_{Sum} , the NCEP results overall were slightly larger than observations, especially between April and July. The simulation from H3A2 and H3B2 had the peak shifted by 1 month from May to June. The seasonal pattern of simulated $E_{90Percentile}$, E_{Max} , and E_{Max5_tot} were similar, e.g., an overestimation in summer and an underestimation in later spring. In general, the results were acceptable for practical use.

4.2.3 Precipitation

Daily precipitation at a station or at a local scale is the pivotal input variable to a rainfall-runoff model and plays a

cumulative pan evaporation (E_{Max5_Tot}) between observed and generated values in the validation period (1984–1993)

critical role in the study of climate change impact on hydrological systems (Chen et al. 2006). Furthermore, both the rain occurrence and the amount of precipitation are stochastic processes; therefore, the downscaling of precipitation is always a difficult problem (Doyle 1997).

It can be seen in Fig. 5 that the simulated mean monthly precipitation was broadly lower, especially in the rainy season of June and July except for P_{90Pop} and P_{90Pop_Tot} . Therefore, we can deduce that the high rainfall and concentrated period precipitation cannot be well captured by the model. The overestimation of P_{Max} in June was because Beijing, Tianjin, and Zunhua stations had recorded rain as high as 139.2, 130.5, and 69.1 mm/day, respectively, on 27 June, 1986. The return period of this rainfall in June in Beijing and Tianjin was estimated to be about 50 years. In addition, Chengde and Tanggu had 40 return period storms on 1991.6.8 and 1984.6.15, with rainfall of 79.1 and 121.3 mm/day, respectively. The abnormal amount of storm rainfall at these five stations contributed to the high value of area-average precipitation in June. Since the validation period only had 10 years, the simulation could not accurately reflect the abnormal storm events. As to the $P_{90Percentile}$, the simulation was generally underestimated, and the underesti-

Fig. 5 Comparison of **a** Total amount of monthly precipitation (P_Sum), **b** Maximum 1-day precipitation on wet days (P_Max), **c** Maximum 5-day precipitation on wet days (P_Max5_Tot), **d** 90% quantile of daily precipitation on wet days ($P_90Percentil$), **e** Number of days with precipitation exceeding the 90% quantile (P_90Pop), **f** Percentage of precipitation at days with more than 90% quantile (P_90Pop_Tot), **g** Percentage of wet days ($Wet_Day\%$) and **h** Maximum length of continuous dry-spell (Max_Dspel) between observed and generated values in the validation period (1984–1993)

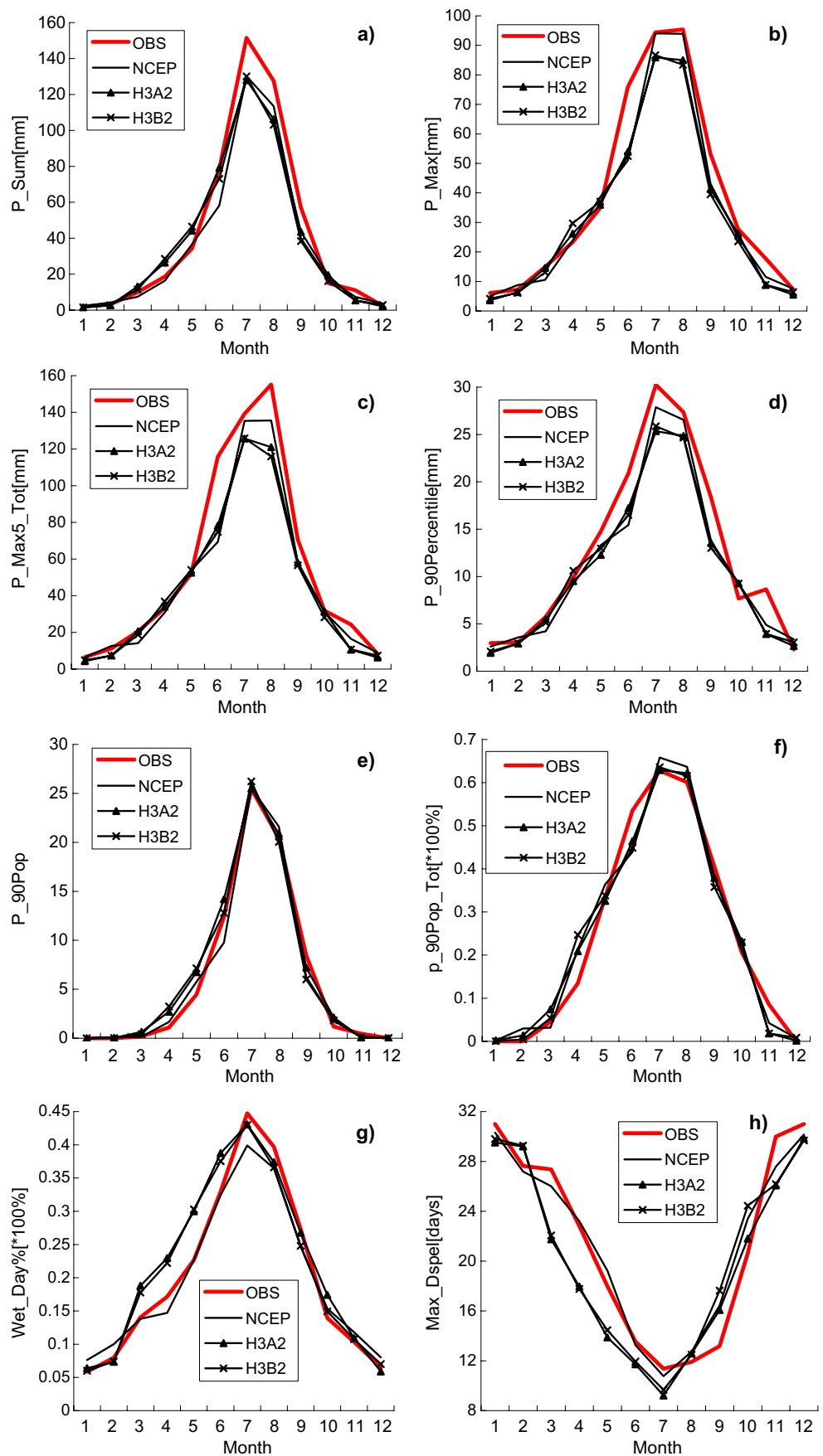


Table 4 Comparison of the difference of statistical indices of mean temperature between current (1971–2000) and future climate (2011–2040) conditions

	T_Mean		T_Max		T_Min		T_Max5_Tot	
	A2(F-C)	B2(F-C)	A2(F-C)	B2(F-C)	A2(F-C)	B2(F-C)	A2(F-C)	B2(F-C)
DJF	0.508	0.535	1.691	0.920	0.921	-0.456	12.032	9.209
MAM	0.383	0.736	1.234	1.472	1.262	-0.527	0.233	5.129
JJA	0.544	0.679	0.266	-0.278	0.506	2.516	2.589	0.047
SON	0.985	1.136	0.848	2.483	-0.109	-1.437	3.751	11.156
Annual	0.605	0.771	0.278	-0.249	0.921	-0.456	2.588	0.079

The meanings of four statistical indices are same as showed in the caption of Fig. 3

mation was most obvious in summer with the results from H3A2 and H3B2. The measured P_90Percentile was abnormally high in November; from the historical data, it was found that the P_90Percentile at coastal stations, such as Baoding, Langfang, Tianjin, and Tanggu stations, was significantly higher than at other stations in November, with the amount being up to 10 mm/day, while other stations had a rainfall of 4–8 mm/day. Due to the marine lag effect, the temperature at these stations was higher in November; the cold air from inland to Bohai Sea meets the warm air from ocean and form clouds and local rain events. As to the P_90Pop and P_90Pop_Tot, the simulated rain occurrence and amount were accurate by and large. As to the wet-day%, the simulated results from NCEP data were similar to the measured values, except for an underestimation in July and August. The simulated values with H3A2 and H3B2 were systematically larger in the first half of the year while accurate in the second half of the year. Consequently, for the Max_Dspel, the simulation from H3A2 and H3B2 was underestimated in the first half of the year and an overestimation occurred in autumn, especially in September.

A close look at the historical measured data reveals that the Max_Dspel of stations along Taihang Mountain and Yan Mountain, such as Weixian, Huailai, Zhangjiakou, Fengning, and Chengde, were much smaller than other stations in September, with dry spell being about 9 or 10 days, which can be attributed to the orographic rainfall when warm and humid airflow climbed the mountain and blocked by the mountains. Therefore, SDSM has some limitation in simulating the rainfall affected by special terrains. Above all, SDSM can quite accurately reflect the total amount of precipitation and seasonal change patterns,

although this method also has some limitation in simulating the orographic rainfall. In conclusion, underestimation of the total amount and some extreme values to some extent can be attributed to the short validation period which is heavily influenced by some extreme events appearing in the record with a return period much larger than that in the validation period.

4.3 Downscaling daily mean temperature, pan evaporation, and precipitation under future emission scenarios

According to worldwide rule, the spell of 1971–2000 was taken as the current climate (C), and the spell of 2011–2040 was taken as the near future predicted climate (F) in this study. The patterns of change about mean temperature, pan evaporation, and precipitation were then analyzed, using only H3A2 and H3B2 data. The downscaled results for the current climate and the difference between the current and future climate change are shown in Tables 4, 5, and 6.

4.3.1 Mean temperature

From Table 4, it can be seen that when compared with current climate, the mean temperature would increase by about 0.7°C in the next 30 years. The most warming amplitudes may happen in autumn and slightly decrease in winter and keep basically the same in spring and summer. In the future, the T_Max and T_Max5_Tot would largely increase, especially in autumn, and the increase with H3B2 would be more than with H3A2. As to the future T_Min, the simulated values would be lower in H3B2 but higher

Table 5 Comparison of the difference of statistical indices of pan evaporation between current (1971–2000) and future climate (2011–2040) conditions

	E_Sum		E_Max		E_90Percentile		E_Max5_Tot	
	A2(F-C)	B2(F-C)	A2(F-C)	B2(F-C)	A2(F-C)	B2(F-C)	A2(F-C)	B2(F-C)
DJF	-4.057	-5.072	-0.023	-0.129	-0.109	-0.086	-0.813	-0.769
MAM	13.016	-13.432	0.097	-0.489	0.201	-0.231	0.078	-1.542
JJA	31.443	0.541	0.541	0.012	0.557	0.072	2.346	-0.656
SON	2.814	-8.881	0.300	-0.164	0.097	-0.175	1.611	-1.055
Annual	43.081	-27.013	0.442	-0.134	0.347	-0.068	2.052	-0.812

The meanings of four statistical indices are same as showed in the caption of Fig. 4

Table 6 Comparison of the difference of statistical indices of precipitation between current (1971–2000) and future climate (2011–2040) conditions

	P_Sum		P_Max		P_Max5_Tot		P_90Percentile		P_90Pop		P_90Pop_Tot		Wet_Day%		Max_Dspel	
	A2(F-C)	B2(F-C)	A2(F-C)	B2(F-C)	A2(F-C)	B2(F-C)	A2(F-C)	B2(F-C)	A2(F-C)	B2(F-C)	A2(F-C)	B2(F-C)	A2(F-C)	B2(F-C)	A2(F-C)	B2(F-C)
DJF	1.641	1.849	-0.136	1.704	0.033	2.522	0.193	0.162	-0.023	0.086	-0.004	0.004	0.011	0.011	-7.318	-7.495
MAM	-5.970	-1.597	-5.845	-4.001	-8.954	-4.934	-0.198	-0.305	-1.564	-2.214	0.002	-0.015	-0.011	0.002	0.000	0.309
JJA	-23.258	11.206	-3.854	1.156	-3.354	7.495	-0.121	0.560	-7.482	5.973	0.014	0.008	-0.025	0.005	1.091	0.418
SON	-2.518	6.760	0.978	7.586	-0.796	7.844	-0.060	0.430	0.286	3.150	0.009	0.014	-0.007	0.007	1.405	0.673
Annual	-30.050	18.280	-4.003	2.548	-3.386	7.710	-0.498	0.108	-8.782	6.995	0.006	0.003	-0.008	0.007	-3.445	-4.014

The meanings of eight statistical indices are same as showed in the caption of Fig 5

than in H3A2 when compared to the current climate and would decrease more in autumn. Above all, in the future, the T_Mean would increase, and extreme events would be more obvious, and the largest amplitude of change would happen in autumn.

4.3.2 Pan evaporation

In Table 5, it can be seen that the change trend of H3A2 and H3B2 is different; the pan evaporation in H3A2 would increase in spring, summer, and autumn, while decrease in winter, and H3B2 had no change; on average, the annual pan evaporation amount would increase by about 8 mm, and the more increase would happen in summer. In the future, the E_Max had no much obvious change; the E_90Percentile would also increase in the future and mainly concentrated in summer. In conclusion, the change pattern of pan evaporation was not very clear in the future.

4.3.3 Precipitation

It is shown clearly in Table 6 that the annual amount of precipitation would decrease by about 7% in H3A2 while increase by about 4% in H3B2, and the change was mainly found in summer. In winter, there was an increase in both A2 and B2 scenarios. In the future, the P_Max and P_Max5_Tot would have little decrease in A2 but increase in B2, especially in autumn. In the future, the threshold of storm (P_90Percentile) had no remarkable change. As to the storm occurrence (P_90Pop), the number of days would decrease by about 9 days in A2 while increase by about 7 days in B2, especially in summer. When it came to the P_90Pop_Tot, there was no obvious variation. In the future, the change of wet-day% could be neglected. As for the Max_Dspel, it would basically become shorter, especially in winter. Above all, when compared with the current climate, the amount of precipitation would largely decrease; the maximum spell of dry-day would become shorter; rain occurrence had no significant change; the intensity of extreme precipitation event as measured by P_Max and P_Max5_Tot could be strengthened in B2, while weakened in A2.

5 Conclusions

Statistical downscaling methods are effective measures to fill the gap between large-scale climate change and local-scale hydrological response; among them, SDSM is widely used for its simplicity and superior capability. In this study, SDSM is applied to the Haihe River basin, China, and we investigated its applicability by downscaling mean temperature, pan evaporation, and precipitation, which are impor-

tant for assessing the impact of climate change on water resource management. Furthermore, we analyzed their patterns of change for 2011–2040, which would pave the way for the study of hydrological impacts under future climate change in the Haihe River basin.

It is a big challenge to select predictors under the strong influence of East Asia monsoon and complex climate conditions. We found that different sets of predictors to different predictands can be selected from a wide space by using the SMLR method, and these predictors have some physical meaning. As to the mean temperature, it is more sensitive to the near surface atmospheric variables, the airflow from northwest is transferred mainly by vorticity and horizontal wind, and the southeast airflow is affected mainly by sea surface mean pressure. As to the pan evaporation, northern zonal wind at 500 hPa level and humidity in central and middle part would have influence; as far as precipitation is concerned, in the north, it is mainly affected by meridional airflow above 700 hPa and horizontal airflow below 700 hPa, and in the south it is mainly influenced by the vorticity at 850 hPa level.

Calibrating and validating SDSM with the NCEP reanalysis data selected by the SMLR method have proven to be successful, and the amount and the pattern of change can be simulated well. The best result is the mean temperature with R^2 equal to 99%, followed by pan evaporation with R^2 between 87% and 96%, and precipitation with R^2 equal to about 73%. The simulation from H3A2 and H3B2 is worse than that from NCEP data in the validation period, partly because SDSM is fitted using the NCEP data. Above all, using selected predictors from the SMLR method and feeding them to SDSM, the variation characteristic of mean temperature, pan evaporation, and precipitation can be reasonably produced, and this method is adaptable in the Haihe River basin.

It is concluded that the T_{Mean} can be accurately simulated; however, the result from H3A2 and H3B2 has systematic errors in simulating extreme events; it can overestimate high values and underestimate low values. In the next 30 years from 2011 to 2040, the temperature extreme events would be more significant, especially in autumn.

In the future, the change pattern of pan evaporation is not obvious since the factors working on evaporation are complicated.

The amount of precipitation and the pattern of seasonal change in storms can be better simulated; however, the extreme events in July and August can be underestimated; it is partly because the abnormal condition caused by special terrain and special weather events appear in the validation period. When compared with current climate, the total amount of precipitation would largely decrease; the maximum spell of dry-day would be shortened,

especially in winter; the intensity of extreme precipitation events would be augmented in B2 scenario while weakened in A2 scenario.

Although SDSM and the SMLR method can well simulate mean values and trend of changes, however, they have limitations in special terrains and in conditions affected by special local weather events. Their simulation capacity in producing extreme events needs to be validated further, so it calls for the lengthening of the observation data time series on one hand and the improvement of the model itself on the other hand.

Acknowledgments The authors wish to thank Dr. Li, H.Q. for providing preparation knowledge to statistical downscaling and SDSM method and Dr. Ji, D.Y. and Pan, X.Y. for valuable discussion during work. This study was supported by the Key Project of International Cooperation of the Natural Science Foundation of China (No. 40730632); The Special Fund of Ministry of Science and Technology, China (No. 2006DFA21890); and The Knowledge Innovation Key Project of the Chinese Academy of Sciences (No. Kzcx2-yw-126).

References

- Bardossy A, Plate EJ (1992) Space-time model for daily rainfall using atmospheric circulation patterns. *Water Resour Res* 28(5):1247–1259
- Burger G, Chen Y (2005) Regression-based downscaling of spatial variability for hydrologic applications. *J Hydrol* 311:299–317
- Busuioac A, Von Storch H, Schnur R (1999) Verification of GCM-generated regional seasonal precipitation for current climate and of statistical downscaling estimates under changing climate conditions. *J Climate* 12:258–272
- Chen DL (2000) A monthly circulation climatology for Sweden and its application to a winter temperature case study. *Int J Climatol* 20:1067–1076
- Chen X, Chen YQ (2001) Downscaling of daily precipitation using a stochastic weather generator. *J Hydraul Eng* 4:47–52 (in Chinese with English abstract)
- Chen YD, Chen X, Xu C-Y, Shao Q (2006) Downscaling of daily precipitation with a stochastic weather generator for the subtropical region in South China. *Hydrol Earth Syst Sci Discuss* 3:1145–1183
- Coulibaly P (2004) Downscaling daily extreme temperatures with genetic programming. *Geophys Res Lett* 31:L16203. doi:10.1029/2004GL020075
- Cubasch U, Von Storch H, Waszkewitz J, Zorita E (1996) Estimates of climate change in Southern Europe derived from dynamical climate model output. *Clim Res* 7:129–149
- Dibike YB, Coulibaly P (2005) Hydrologic impact of climate change in the Saguenay watershed: comparison of downscaling methods and hydrologic models. *J Hydrol* 307:145–163
- Doyle JD (1997) The influence of mesoscale orography on a coastal jet and rainband. *Mon Weather Rev* 125(7):1465–1488
- Eric P, Salathe JR (2003) Comparison of various precipitation downscaling methods for the simulation of streamflow in a rainshadow river basin. *Int J Climatol* 23:887–901
- Fan LJ (2006) Statistical downscaling of local and regional climate scenarios over China. PhD thesis. Beijing: Institute of Atmo-

- spheric Physics, Chinese Academy of Sciences. 2-3. (in Chinese with English abstract)
- Fan ZQ, Liu CZ (1992) Analysis on the processed of water vapor transfer over North China during 1980–1987. *Sci Atmos Sin* 16(5):548–555 (in Chinese with English abstract)
- Fan LJ, Fu CB, Chen DL (2005) Review on creating future climate change scenarios by statistical downscaling techniques. *Adv Earth Sci* 20(3):320–329 (in Chinese with English abstract)
- Fan LJ, Fu CB, Chen DL (2007) Estimation of local temperature change scenarios in North China using statistical downscaling method. *Chin J Atmos Sci* 31(5):887–897 (in Chinese with English abstract)
- Fowler HJ, Wilby RL (2007) Beyond the downscaling comparison study. *Int J Climatol* 27:1543–1545
- Fowler HJ, Blenkinsop S, Tebaldi C (2007) Linking climate change modelling to impacts studies: recent advances in downscaling techniques for hydrological modelling. *Int J Climatol* 27:1547–1578
- Frias MD, Zorita E, Fernandez J, Rodriguez-Puebla C (2006) Testing statistical downscaling methods in simulated climates. *Geophys Res Lett* 33:L19807. doi:10.1029/2006GL027453
- Hanssen-Bauer I, Achberger C, Benestad RE, Chen DL, Forland EJ (2005) Statistical downscaling of climate scenarios over Scandinavia. *Clim Res* 29:255–268
- Harpham C, Wilby RL (2005) Multi-site downscaling of heavy daily precipitation occurrence and amounts. *J Hydrol* 312:235–255
- Hayhoe K, Cayan D, Field CB, Frumhoff PC, Maurer EP, Miller NL, Moser SC, Schneider SH, Cahill KN, Cleland EE, Dale L, Drapek R, Hanemann RM, Kalkstein LS, Lenihan J, Lulich CK, Neilson RP, Scheridan SC, Verville JH (2004) Emissions pathways, climate change, and impacts on California. *Pnas* 101(34):12422–12427
- Hellstrom C, Chen DL, Achberger C, Ralsanen J (2001) Comparison of climate change scenarios for Sweden based on statistical and dynamical downscaling of monthly precipitation. *Clim Res* 19:45–55
- IPCC (2007) Climate Change 2007: the physical science basis. In: Solomon S, Qin D, Manning M, Chen Z, Marquis M, Averyt KB, Tignor M, Miller HL (eds) Contribution of Working Group I to the Fourth Assessment Report of the Intergovernmental Panel on Climate Change. Cambridge University Press, Cambridge
- Kang HW, An KH, Park CK, Solis ALS, Stitthichivapak K (2007) Multimodel output statistical downscaling prediction of precipitation in the Philippines and Thailand. *Geophys Res Lett* 34:L15710. doi:10.1029/2007GL030730
- Khan MS, Coulibaly P, Dibike Y (2006) Uncertainty analysis of statistical downscaling methods. *J Hydrol* 319:357–382
- Kite GW (1997) Simulating Columbia river flows with data from regional-scale climate models. *Water Resour Res* 33(6):1275–1285
- Liao YM, Zhang Q, Chen DL (2004) Precipitation simulation in China with a weather generator. *Acta Geogr Sin* 59(5):689–698 (in Chinese with English abstract)
- Liu LL, Liu ZF, Xu ZX (2008) Trends of climate change for the upper-middle reaches of the Yellow River in the 21st century. *Adv Clim Chang Res* 4(3):167–172 (in Chinese with English abstract)
- Murphy J (2000) Predictions of climate change over Europe using statistical and dynamical downscaling techniques. *Int J Climatol* 20:489–501
- Ren GY (2007) Climate change and China's water resources. China Meteorological Press, Beijing (in Chinese)
- Richardson CW (1981) Stochastic simulation of daily precipitation, temperature, and solar radiation. *Water Resour Res* 17(1):182–190
- Risbey JS, Stone PH (1996) A case study of the adequacy of GCM simulations for input to regional climate change assessments. *J Climate* 9:1441–1467
- Samel AN, Wang WC, Liang XZ (1999) The monsoon rainband over China and relationships with the Eurasian circulation. *J Climate* 12:115–131
- Shi YF (1995) The impact of climate change on the water resources in West and North China. Science and Technology Publishing House, Shandong (in Chinese)
- Tripathi S, Srinivas VV, Nanjundiah RS (2006) Downscaling of precipitation for climate change scenarios: A support vector machine approach. *J Hydrol* 330:621–640
- Von Storch H, Zorita E, Cubasch U (1993) Downscaling of global climate change estimates to regional scales: an application to Iberian rainfall in wintertime. *J Climate* 6:1161–1171
- Vrac M, Stein ML, Hayhoe K, Liang XZ (2007) A general method for validating statistical downscaling methods under future climate change. *Geophys Res Lett* 34:L18701. doi:10.1029/2007GL030295
- Wang YQ, Leung LR, Mcgregor JL, Wang WC, Ding YH, Kimura F (2004) Regional climate modeling: progress, challenges, and prospects. *J Meteorol Soc Jpn* 82(6):1599–1628
- Wentz FJ, Ricciardulli L, Hilburn K, Mears C (2007) How much more rain will global warming bring? *Science* 317:233–235
- Wetterhall F, Halldin S, Xu C-Y (2005) Statistical precipitation downscaling in central Sweden with the analogue method. *J Hydrol* 306:174–190
- Wetterhall F, Bardossy A, Chen DL, Halldin S, Xu C-Y (2006) Daily precipitation-downscaling techniques in three Chinese regions. *Water Resour Res* 42:W11423. doi:10.1029/2005WR004573
- Wetterhall F, Halldin S, Xu C-Y (2007) Seasonality properties of four statistical-downscaling methods in central Sweden. *Theor Appl Climatol* 87(1–4):123–137
- Wilby RL, Harris I (2006) A framework for assessing uncertainties in climate change impacts: low-flow scenarios. *Water Resour Res* 42:W02419. doi:10.1029/2005WR004065
- Wilby RL, Wigley TML (1997) Downscaling general circulation model output: a review of methods and limitations. *Progr Phys Geogr* 21(4):530–548
- Wilby RL, Wigley TML, Conway D, Jones PD, Hewitson BC, Main J, Wilks DS (1998) Statistical downscaling of general circulation model output: a comparison of methods. *Water Resour Res* 34(11):2995–3008
- Wilby RL, Hay LE, Leavesley GH (1999) A comparison of downscaled and raw GCM output: implications for climate change scenarios in the San Juan River basin, Colorado. *J Hydrol* 225:67–91
- Wilby RL, Dawson CW, Barrow EM (2002) SDSM - a decision support tool for the assessment of regional climate change impacts. *Environ Model Softw* 17:147–159
- Wilby RL, Tomlinson OJ, Dawson CW (2003) Multi-site simulation of precipitation by conditional resampling. *Clim Res* 23:183–194
- Wilks DS (1989) Conditioning stochastic daily precipitation models on total monthly precipitation. *Water Resour Res* 25(6):1429–1439
- Xu C-Y (1999) From GCMs to river flow: a review of downscaling methods and hydrologic modelling approaches. *Progr Phys Geogr* 23(2):229–249
- Yuan F, Xie ZH, Ren LH, Huang Q (2005) Hydrological variation in Haihe River Basin due to climate change. *J Hydraul Eng* 36(3):274–279 (in Chinese with English abstract)
- Zhao FF, Xu ZX (2008) Statistical downscaling of future temperature change in source of the Yellow River Basin. *Plateau Meteorol* 27(1):153–161 (in Chinese with English abstract)